RESEARCH ARTICLE

Does a low-pH microenvironment around phototrophic Fe^{II}-oxidizing bacteria prevent cell encrustation by Fe^{III} minerals?

Florian Hegler[1], Caroline Schmidt[1], Heinz Schwarz[2] & Andreas Kappler[1]

[1]Geomicrobiology, Center for Applied Geosciences, University of Tuebingen, Tuebingen, Germany; and [2]Max-Planck Institute for Evolutionary Biology, Tuebingen, Germany

Correspondence: Andreas Kappler, Geomicrobiology, Center for Applied Geosciences, University of Tuebingen, Sigwartstraße 10, D-72076 Tuebingen, Germany. Tel.: +49 7071 297 4992; fax: +49 7071 295 059; e-mail: andreas.kappler@uni-tuebingen.de

Received 31 May 2010; revised 28 August 2010; accepted 12 September 2010.
Final version published online 15 October 2010.

DOI:10.1111/j.1574-6941.2010.00975.x

Editor: Alfons Stams

Keywords
ferrous iron oxidation; biomineralization; mineral precipitation; phototrophic Fe^{II} oxidizers.

Abstract

Neutrophilic Fe^{II}-oxidizing bacteria precipitate positively charged Fe^{III} minerals that are expected to sorb to the negatively charged cell surface, leading to encrustation and thus limiting the cells' accessibility to substrates and nutrients. However, electron-microscopy analysis of phototrophic iron-oxidizing *Thiodictyon* sp. strain F4 cells showed no encrustation, but mineral precipitation at a distance from the cell surface. *In situ* fluorescence microscopy analysis of F4 cells using a pH-sensitive fluorescent dye revealed a low cell surface pH (6.0 ± 0.1) in contrast to the bulk pH (6.6 ± 0.1). Biogeochemical modeling showed that the pH difference reduces Fe^{III} sorption and Fe^{III} precipitation rates at the cell surface, therefore directing mineral formation away from the cells. The results from this study therefore suggest that the establishment of a low cell surface pH could provide a mechanism for photoferrotrophs to successfully prevent Fe^{III} mineral precipitation on the cell surface.

Introduction

While Fe^{II} is relatively soluble at a neutral pH, Fe^{III} preferentially occurs in the solid phase as Fe^{III}_{ppt}, with maximum aqueous concentrations of dissolved Fe^{III} [Fe^{III}_{aq}] of approximately 1×10^{-10} mol L^{-1} (Stumm & Morgan, 1995). Iron(III) (oxy)hydroxides [Fe^{III}_{ppt}] are produced chemically and biologically in the environment (Emerson, 2000; Ehrlich & Newman, 2009) by microbial and chemical iron(II) [Fe^{II}] oxidation at a neutral pH (Widdel *et al.*, 1993; Hafenbradl *et al.*, 1996; Straub *et al.*, 1996; Emerson, 2000; Canfield *et al.*, 2005). The phenomenon of microbial Fe^{II} oxidation was discovered already in the early days of microbiology in the 19th century (Ehrenberg, 1836; Winogradsky, 1888). At that time, though, the interaction of iron(III) oxides [Fe^{III} oxides] with bacteria could only be observed visually, but neither the corresponding metabolism nor the underlying mechanism could be explained.

While aerobic neutrophilic Fe^{II} oxidizers *Gallionella* and *Leptothrix* thrive at low concentrations of oxygen, phototrophic Fe^{II} oxidizing bacteria, as well as nitrate-reducing Fe^{II} oxidizers, convert Fe^{II} under anoxic conditions. Fe^{II}-oxidizing bacteria can access the dissolved substrate (Fe^{II}_{aq}) easily at circumneutral pH. However, under such pH conditions, the cells may be harmed by the poorly soluble product (Fe^{III}_{ppt}) of their metabolism because Fe^{III}_{aq} as well as the positively charged Fe^{III}_{ppt} strongly sorb to the negatively charged bacterial cell surfaces. Consequently, cells are expected to encrust with Fe^{III}_{ppt}, leading to a limited exchange of metabolites with their environment. In particular, the Fe^{II}-oxidizing nitrate-reducing *Acidovorax* sp. strain BoFeN1 was shown to encrust heavily with Fe^{III}_{ppt} at circumneutral pH (Miot *et al.*, 2009a; Schaedler *et al.*, 2009).

In this study, we focus on a photoferrotrophic strain that oxidizes Fe^{II} according to the following equation (Widdel *et al.*, 1993):

$$4Fe^{2+} + h\nu + HCO_3^- + 10H_2O \rightarrow 4Fe(OH)_3 + \langle CH_2O \rangle + 7H^+ \quad (1)$$

It has been shown that all electrons stemming from Fe^{II} oxidation are used by phototrophic Fe^{II}-oxidizing bacteria for CO_2 fixation and thus biomass generation (Widdel *et al.*, 1993). Recently, it was suggested for two different strains of

phototrophic Fe^{II}-oxidizing bacteria that the oxidation of Fe^{II} occurs in the periplasm of the cells (Croal *et al.*, 2007; Jiao & Newman, 2007). In contrast to chemotrophic Fe^{II}-oxidizing strains, none of the known photoferrotrophs encrusts with Fe^{III} minerals (Miot *et al.*, 2009b; Schaedler *et al.*, 2009). It is particularly essential for phototrophic Fe^{II}-oxidizing strains to avoid cell encrustation as the mineral coatings may not only limit the exchange of nutrients and metabolites of the cell with its environment. Additionally, the amount of light available for photosynthesis decreases due to the mineral crust and therefore reduces the overall energy available to the cell.

Various mechanisms have been suggested to explain why some Fe^{II}-oxidizing strains do not encrust: (1) organic exopolymers, similar to those observed for *Gallionella* spp., could help to localize precipitation away from the cell (Chan *et al.*, 2009; Schaedler *et al.*, 2009 and references therein). Still, this mechanism does not explain why the Fe^{III}_{aq} released does not immediately bind to the negatively charged cell surface after Fe^{II} oxidation. (2) Shedding of parts of the cell surface covered with Fe precipitates could remove the precipitates from the surface (Emerson & Revsbech, 1994). (3) Fe^{III} complexation by organic ligands allows Fe^{III} to remain in solution and prevents precipitation (Croal *et al.*, 2004a). However, in the case of autotrophic organisms, CO_2 reduction for the synthesis of such ligands is quite costly in terms of the Fe requirement. Four atoms of Fe^{II} have to be oxidized to reduce a single CO_2 to biomass (e.g. usable in a complexing molecule keeping Fe^{III} in solution) Eqn. (1). Several carbon atoms are usually required per ligand. For example, 36 Fe^{II} would have to be oxidized to produce a single ligand molecule with six carbon atoms (with a C oxidation state of 0) and this carbon would not be available for cell biomass while it could complex only one Fe^{III} atom. Organic ligands (such as oxalate) requiring very few electrons for their synthesis from CO_2 could potentially be suitable as complexing agents. However, although oxalic acid would fulfill this requirement by needing only two electrons to be synthesized from two CO_2 molecules, an effective recycling of any of these ligands is unlikely, mainly due to the photoreactivity of many organic Fe^{III} ligands, leading to the degradation of the ligands (Barbeau *et al.*, 2001). Therefore, this mechanism does not seem to be very plausible. (4) The amount of negatively charged (and therefore Fe^{III} binding) functional groups on the cell surface could be reduced or the cell surface charge could even be reversed from negative to positive to avoid primary precipitation (Beveridge & Murray, 1980; Urrutia Mera *et al.*, 1992). This has been shown only for cyanobacteria (McConnaughey & Whelan, 1997; Martinez *et al.*, 2010), but it is unknown whether photoferrotrophs are also able to change their surface charge. (5) Fe^{III} precipitation at the cell surface could be delayed, lowered or even prevented by acidifying the cell microenvironment (Sobolev & Roden, 2001; Kappler & Newman, 2004; Schaedler *et al.*, 2009).

An environment of enhanced proton activity around the cell (termed 'low-pH microenvironment' in this study) has the advantage for a cell that it does not require additional biomass to be produced for the complexation of Fe^{III} by organic ligands, shedding of parts of the cell or localization of precipitates on exopolymers (e.g. stalks). In the case of phototrophic Fe^{II}-oxidizing bacteria, acidification around colonies of cells has been observed previously (Kappler & Newman, 2004). However, it is unclear whether this acidification stems from the formation of $Fe(OH)_3$ from Fe^{3+}_{aq} that would release protons [according to Eqn. (1), where Fe^{II} oxidation is coupled to CO_2 fixation] or whether the lower pH was actively caused by the cells via proton translocation.

Therefore, the objectives of this study were (1) to analyze the pH at the single-cell level compared with the bulk medium using the phototrophic Fe^{II}-oxidizing bacterium *Thiodictyon* sp. F4, a gram-negative, γ-proteobacterium (Croal *et al.*, 2004b), and (2) to evaluate whether and how the establishment of a single-cell pH-microenvironment influences Fe^{III} sorption and Fe^{III} mineral precipitation. Micrometer pH measurements were achieved using a combination of confocal laser scanning microscopy (CLSM) and a pH-dependent fluorescent dye. Geochemical modeling was used to determine the pH dependence of Fe^{III} sorption and precipitation and to evaluate whether an actively sustained pH microenvironment might prevent encrustation.

Materials and methods

Medium, chemicals and growth conditions

The phototrophic Fe^{II} oxidizer *Thiodictyon* sp. strain F4 (Croal *et al.*, 2004b) was grown in a mineral medium buffered with 22 mM bicarbonate at pH 6.8–6.9. The addition of 10 mM $FeCl_2$ as electron donor decreased the pH slightly to pH 6.6. For a detailed description of the growth conditions, see Hegler *et al.* (2008). The fluorescent dye SNARF®-4F 5-(and-6)-carboxylic acid (SNARF4F) (Invitrogen, 2003; Marcotte & Brouwer, 2005) by Molecular Probes® was dissolved in water (2 mM) and aliquots were frozen and used not longer than 4 months to avoid the potential hydrolytic degradation of the dye. Samples of *Thiodictyon* sp. strain F4 cultures were taken at the end of the exponential growth phase and 500 μL of the sample was mixed with 1 μL of the dye solution in an anoxic glovebox (100% N_2) in order to avoid oxygen exposure (final concentration of the dye: 4 μM). Although some association of the dye and the cell wall may occur, we chose this dye because it does not penetrate the cell itself (Invitrogen, 2003). The potential association of the dye with the cell

surface was not expected to affect its pH-dependent fluorescence (Invitrogen, 2003).

Microscopic analysis of a single-cell pH microenvironment

An oxygen-tight microscopy chamber covered with a coverslip was used to avoid physical pressure to the minerals and to maintain the sample anoxic during microscopy. The chambers were prepared by gluing a coverslip onto the microscopy slide with epoxy-based glue (Uhu plus schnellfest; UHU GmbH & Co. KG, Germany) including two syringe needles as the inlet and the outlet. They were washed with double-distilled water before use.

The chambers were filled with the culture/dye mixture and incubated for 45 min before microscopic analysis at light saturation. This duration of time allows CCCP to deenergize the membranes. As it was recently suggested that Fe^{II} oxidation occurs in the periplasm of phototrophic Fe^{II}-oxidizing bacteria (Croal *et al.*, 2007; Jiao & Newman, 2007), no active (energy-requiring) uptake of Fe^{II} into the cytoplasm is needed and therefore Fe^{II} oxidation did not stop immediately after the addition of CCCP. However, reducing equivalents accumulate due to the oxidation of Fe^{II}, but cannot be reoxidized; hence, finally, Fe^{II} oxidation will stop due to the lack of electron acceptors.

Microscopy was performed on a Leica TCS SP2 confocal scanning laser microscope. The dye was excited at 488 nm, and the fluorescence was measured at emission wavelengths of 580–590 and 650–660 nm (Fig. 1a–c). The ratio of the two wavelengths was used to calculate the pH according to a calibration curve. Continuous spectra for dye calibration were measured in 20 mM PBS buffer with a pH between 5 and 7.5 using a Jena Analytics FlashScan 550 fluorescence plate reader at an excitation of 488 nm. The ratio between the individual wavelengths (580–590 and 650–660 nm) was calculated depending on the pH. We fitted the curve to account for the nonlinear parts away from the pK_a of the

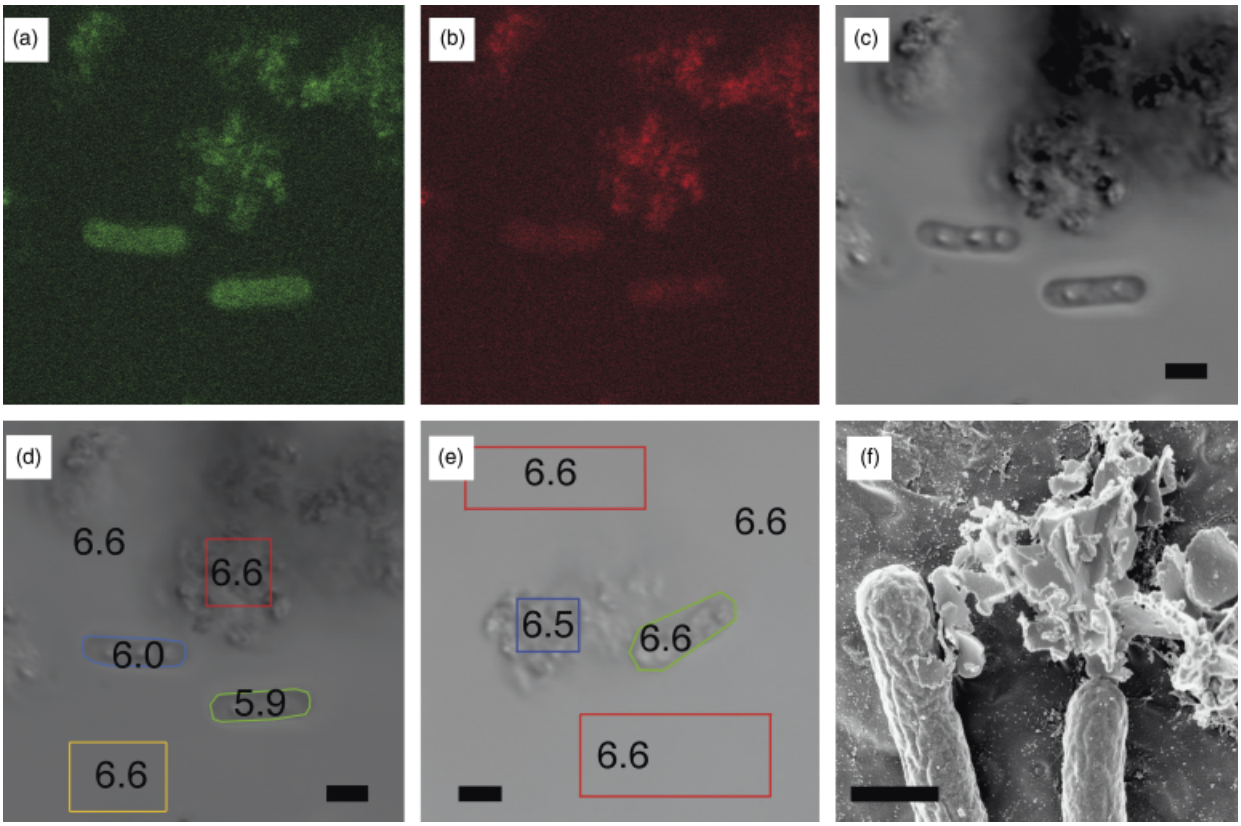

Fig. 1. Confocal laser scanning microscopy (CLSM) imaging of *Thiodictyon* sp. F4 cells stained with a pH-dependent fluorescent dye, demonstrating the presence of a cell pH microenvironment. (a–c) CLSM pictures of cells stained with SNARF4. (a) 580–590 nm, (b) 650–660 nm, (c) gray-scale image. The ratio of (a)/(b) allows calculating the pH. (d) pH microenvironment around cells of *Thiodictyon* sp. F4, the pH was 6.6 ± 0.1 in the background (yellow box) and mineral (red box), bulk measurements with a pH electrode confirmed the values determined with the pH-dependent dye. The pH at the cell level was 5.9 ± 0.1 (green cell) and 6.0 ± 0.1 (blue cell). (e) Red, background; green, cell; blue, mineral, CCCP used to decouple the proton gradient. The pH was 6.6 ± 0.1 at the cell level, the background also had pH 6.6 ± 0.1 for both areas, the pH at the mineral was 6.5 ± 0.1 while the entire frame had a pH of 6.6 ± 0.1. Bulk measurements with a pH electrode confirmed these values. Scale bar = 2 μm in all images (a)–(e). (f) Scanning electron micrograph of *Thiodictyon* sp. F4, scale bar = 1 μm. The cell is associated with Fe^{III} minerals, but not encrusted.

dye. The ratio between the individual wavelengths and its correlation to the pH was used to calculate the pH values in the microscopy images.

In order to determine whether the establishment of the ΔpH in the cell microenvironment is an active or a passive process, carbonyl cyanide 3-chlorophenylhydrazone (CCCP; Sigma Aldrich, Germany) was used – a protonophore that decouples the proton-motive force (PMF) across the membrane (Harold, 1972).

Electron microscopy

For scanning electron microscopy, samples were prepared as described previously (Schaedler *et al.*, 2008).

Calculation of the Fe^{II} oxidation rate per cell

In order to calculate the amount of Fe^{II} oxidized per cell per unit time, we quantified the decrease of total Fe^{II} over time as described previously (Hegler *et al.*, 2008). Additionally, cells were counted microscopically: 1 mL culture was fixed with glutaraldehyde (final concentration of 2.5%), followed by the dissolution of the minerals at pH 3 with oxalic acid (15 g L^{-1}) and oxalate (28 g L^{-1}). After the dissolution of the Fe^{III}_{ppt} and staining of the cells with 4′,6-diamidino-2-phenylindol (DAPI), a subsample was passed through a Nucleopore-filter (0.22 μm pore size, Millipore) and the amount of cells per filter area was counted in an epi-fluorescence microscope. The data allowed calculating the maximum Fe^{III} production rates per cell, which were used for calculating the sorption of Fe^{III} onto the cell surface. The bulk Fe^{III} formation rate was determined by following Fe^{II} oxidation over time (which is equal to Fe^{III} formation) and calculating the turnover in the entire culture over the complete oxidation phase of 218 h. The release of Fe^{III} per second was calculated to be 4.3×10^{-7} mM s^{-1}.

Modeling

The resolution of the microscope did not allow resolving the expected pH gradient between the cell surface and the bulk medium. Thus, a gradient of proton activity was interpolated between the cell surface and the bulk medium for modeling. Additionally, geochemical modeling was applied to evaluate the sorption of ferric iron to the cell surface. Unfortunately, cell surface titrations could not be used to quantify the different functional groups involved in mineral sorption processes at the cell surface of the Fe^{II}-oxidizing strain because the Fe^{III} minerals (produced during Fe^{II} oxidation) interfered with the titrations. Microscopic analysis revealed (data not shown) that dissolving the minerals killed the cells, partially destroyed the cell integrity and increased the number of (titratable) functional groups originating from the cell interior, likely falsifying the titration measurements. Additionally, sorption of Fe^{III} ions to cell surfaces cannot be quantified directly at circumneutral pH due to the low solubility of the Fe^{III} at this pH.

However, it has been shown that as an alternative approach, a general model for site densities and pK_a values can be used to model the adsorption of metals to cell surfaces (Fein *et al.*, 2001). Yee & Fein (2003) showed that the adsorption behavior of different physiological and phylogenetic groups of bacteria, gram-positive as well as gram-negative, and cell mixtures is very similar for various metals. The most abundant cell surface moieties are carboxyls (Borrok *et al.*, 2004). Other functional groups such as protonated amines deprotonate at pH values well above 7 and are thus positively charged at circumneutral pH values. Following the approach of Yee & Fein (2003), we quantified the cell surface interaction of Fe^{3+}_{aq} with the most abundant functional group (carboxyl group).

Calculation of Fe^{III} solubility

Geochemists Workbench 6.04 by Rockware® was used to calculate the speciation and thus the solubility of Fe^{III} in the medium. A matrix including all the chemical compounds present in the medium was set up, see Table 1. For the thermodynamic equilibrium calculations, the dissolved ferric iron concentration (Fe^{III}_{aq}) was defined as follows (including the most dominant Fe^{III} species):

$$\begin{aligned} Fe^{III}_{aq} = & Fe(OH)^0_3 + Fe(OH)^+_2 + FeHPO^+_4 + Fe(OH)^-_4 \\ & + FeOH^{2+} + FeCO^+_3 + Fe_3(OH)^{5+}_4 \\ & + FeH_2PO^{2+}_4 + Fe_2(OH)^{4+}_2 + FeSO^+_4 + Fe^{3+} + \cdots \end{aligned} \quad (2)$$

Table 1. Settings and concentrations of all the chemical compounds included in the matrix used to calculate the solubility of Fe^{III}_{aq} in mineral medium over the pH range from 6 to 7. The resulting graph depicts all dissolved Fe^{III}_{aq} species (Fig. 2)

Component added	
1 kg H_2O	
4.4 mmol L^{-1} $H_2PO^-_4$	Swap $H_2PO^-_4$ for PO^{3-}_4
22 mmol L^{-1} HCO^-_3	Swap HCO^-_3 for CO^{2-}_3
0.68 mmol L^{-1} Ca^{2+}	
4.4 mmol L^{-1} K^+	
2 mmol L^{-1} Mg^{2+}	
22 mmol L^{-1} Na^+	
30.2 mmol L^{-1} Cl^-	
2 mmol L^{-1} SO^{2-}_4	
6.6 mmol L^{-1} NH^+_4	
10 mmol L^{-1} Fe^{3+}	
1e-50 mmol L^{-1} O_2(aq)	
6.0 pH slide pH to 7.0	
Decouple Fe^{2+} and HS^-	
Suppress H_2S (aq) and $FeHS^+$	
Balance off	

Calculation of iron–cell-surface interaction

The following equation was applied to calculate the sorption of Fe^{III} to the carboxylic groups of the cell surface:

$$[ML] = \frac{[\text{site}_{\max}]K_a K_{ads}\left(\frac{M}{H^+}\right)}{1 + K_a K_{ads}\left(\frac{M}{H^+}\right)} \quad (3)$$

where ML is the ligand–metal complex, K_a is the carboxyl-equilibrium constant, K_{ads} represents the adsorption constant while M is the metal concentration and H^+ the proton concentration; site_{max} gives the maximal surface site concentration. The maximal site concentration (site_{max}) represents approximately the total amount of $-$COOH surface sites at pH > 5.

Here, we briefly derive Eqn. (3) with the already introduced abbreviations: deprotonation of carboxylic groups is described by

$$R - COOH \longleftrightarrow R - COO^- + H^+ \quad (4)$$

Replacing $R-COO^-$ by L^- and $R-COOH$ by L and calculating the deprotonated ligand concentration, L^- yields

$$L^- = \frac{[K_a][L]}{[H^+]} \quad (5)$$

This formula determines the concentration of the deprotonated ligands at the cell surface with respect to pH. The adsorption equilibrium can be expressed by

$$M + L^- \longleftrightarrow LM \quad (6)$$

which can be used to calculate the metal–ligand concentration

$$[ML] = K_{ads}K_a[M][L^-] \quad (7)$$

The substitution of L^- of Eqn. (5) into Eqn. (7) leads to

$$[ML] = \frac{K_{ads}K_a[M][L]}{[H^+]} \quad (8)$$

which – after constraining the maximal sorption with a Langmuir isotherm – yields Eqn. (3). A list of all the parameters used in the calculations is compiled in Table 2.

In the calculations, we did not consider abiotic processes that may initiate or stimulate precipitation such as for example the initial presence of nucleation sites (e.g. by the presence of siderite and vivianite crystallites in the growth medium).

Table 2. Compilation of the parameters used to calculate the sorption of Fe^{III} to carboxylic cell surface functional groups

Parameter	Value	Reference
K_a	1.0×10^{-5}	(10)
K_{ads}	1.0×10^{-4}	(8)
Mol R ($-$COOH per cell)	1.8×10^{-16}	(8)
Cells L^{-1} at maximum oxidation rate	$8.0 \times 10^{+10}$	Measured
Site_{max} (mol L^{-1})	1.44×10^{-5}	Calculated
Fe^{III} production rate (mM s^{-1}) at the bulk	4.3×10^{-7}	Measured

Calculation of the precipitation kinetics of Fe^{III}_{ppt}

For the kinetic precipitation calculation, the same speciation setup (Table 1) was used while the reaction rate constant for precipitation ($k_{precipitation} = 2.0 \times 10^7\ M^{-1}\ s^{-1}$, for comparison reaction rate constant for diffusion $k_{diffusion} = 7.9 \times 10^9\ M^{-1}\ s^{-1}$) was taken from Pham *et al.* (2006). In order to determine the precipitation kinetics, we measured the rate of Fe^{III} production for *Thiodictyon* sp. strain F4 (4.3×10^{-7} mM s^{-1}) in a growth experiment (Table 2). The rate of precipitation at the cell surface (at pH 6.0) and in the bulk (at pH 6.6) was calculated accounting for a constant Fe^{III}_{aq} release of 4.3×10^{-7} mM (per second).

Results and discussion

Absence of encrustation and establishment of a pH microenvironment around phototrophic Fe^{II}-oxidizing *Thiodictyon* sp. strain F4 cells

Scanning electron microscopy showed that cells of the phototrophic Fe^{II}-oxidizing *Thiodictyon* strain sp. F4 do not become encrusted when oxidizing Fe^{II} at neutral pH (Fig. 1). This suggests that this strain might be able to minimize or even avoid the sorption of Fe^{III}_{aq} to the cell surface in order to avoid the precipitation of Fe^{III}_{ppt} on its cell surface. To determine whether a low cell surface pH exists for F4 cells and is possibly involved in preventing cell encrustation, we incubated the cells with a dye that shows pH-dependent variations in fluorescence emission.

We determined the pH in the bulk medium with the fluorescent dye in comparison with the values obtained using a standard pH electrode and obtained a value of 6.6 ± 0.1 using both independent methods. As can be seen in Fig. 1, for most active cells, we detected that the cell surface pH was at least 0.6 ± 0.1 units lower compared to the bulk medium of the phototrophic Fe^{II}-oxidizing strain *Thiodictyon* sp. F4. The same effect was observed for approximately 16 out of 20 investigated cells. However, we even found some cells with a larger shift of 0.8 ± 0.1 pH units between surface and bulk pH, although cells with such a larger pH shift were less frequent (about 10–15% of all cells). A few cells (~10%) showed only a very small pH difference from the bulk pH, possibly representing inactive microbial cells. The cells with the highest and the lowest pH variation were not considered in the subsequent geochemical calculations.

In order to test whether an active cell metabolism is necessary to establish the low cell surface pH, we decoupled the membranes with CCCP, a protonophore (Harold, 1972). As a consequence of the exposure to CCCP, the cells were no

longer able to maintain different proton concentrations on both sides of the membrane. In contrast to the untreated cells, we did not observe a lower cell surface pH of these treated cells (Fig. 1e), suggesting that active cell metabolism is required for establishing and maintaining the observed low cell surface pH.

The measured ΔpH is consistent with the ΔpH values compiled by Padan *et al.* (1981) for the PMF and with the pH values calculated from the differences in the sorption of metals to alive and dead cells using surface complexation constants (Johnson *et al.*, 2007). These authors approximated that the difference in metal sorption between active and inactive cells reflected the decrease in sorption capacity due to a pH decrease of approximately 1 pH unit at the cell surface.

Such pH gradients across cell membranes are utilized, for example for ATP generation or for driving the motor units of flagella (Mitchell, 1979; Nicholls & Ferguson, 2002). In phototrophic organisms, protons and positive charges move outside of the cell driven by light energy during cyclic photophosphorylation, acidifying the periplasm and potentially also the close proximity of a bacterial cell surface. If enough light is present, a single electron can theoretically be used several times in the cyclic electron flow to generate the pH gradient across the membrane by pumping protons and creating a lower pH outside of the cell. For photoferrotrophs, the electrons stem from the oxidation of Fe^{II} and are ultimately used to fix CO_2 and thus produce biomass Eqn. (1). Because continuous pumping of protons out of the cell interior (cytoplasm) to the periplasm would ultimately lead to an increasing internal pH being lethal in the end, the protons necessary for the low pH at the cell surface likely stem – at least to a significant extent – from the hydrolysis of Fe^{3+}_{aq} by H_2O molecules after the release of Fe^{3+}_{aq} from the Fe^{II} oxidase. The hydrolysis leads first to the formation of $[Fe^{III}(OH)(H_2O)_5]^{2+}$ and finally to $Fe(OH)_3$ monomers, which then finally precipitate as Fe^{III} hydroxide minerals.

Effect of the low cell surface pH on the sorption, precipitation and dissolution of Fe^{III}

After oxidation of Fe^{II} by the cell and the release of Fe^{3+}_{aq}, the cation either adsorbs to the negatively charged cell surface functional groups or diffuses away from the cell. The Fe^{II}-oxidizing enzymes likely release Fe^{3+}_{aq} and not a hydrolyzed Fe^{III} species. The interaction of metals and metalloids with cell surfaces can be described as sorption, followed by precipitation of the metal ions as minerals (Beveridge & Murray, 1976). Thus, we calculated the sorption of Fe^{3+}_{aq} (as released initially by the cell) to cell surface functional groups. In the initial adsorption step, metal ions, such as iron, compete directly with protons for binding sites at carboxyl- and phosphoryl-functional groups. Calculations

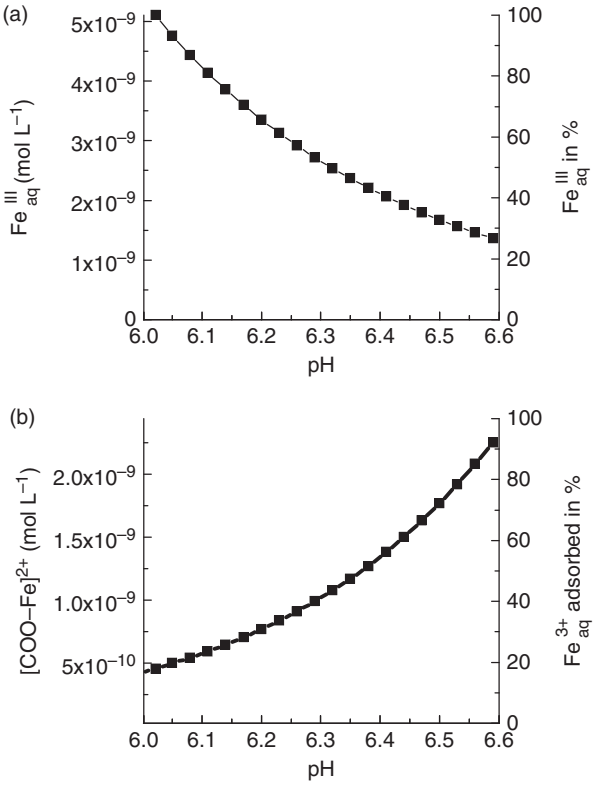

Fig. 2. (a) Change of Fe^{III}_{aq} (in mol L^{-1} and in %) as a function of pH over a range from pH 6.0 to 6.6 based on thermodynamic equilibrium calculations with Geochemists Workbench relative to the Fe^{III}_{aq} concentration at pH 6 that was set to 100% for comparison. (b) Decrease of the initial sorption of Fe^{III} to carboxylic functional groups at the cell surface over the pH range 6.0–6.6. For comparison, sorption at pH 6.6 was set to 100%.

for carboxylic functional groups showed that the sorption of Fe^{3+} to carboxylic surface functional groups decreases by $> 80\%$ with a decline in pH of 0.6 units (Fig. 2). These results agree well with other studies that showed that Co^{2+}, Nd^{3+}, Ni^{2+}, Sr^{2+}, Zn^{2+} (Fein *et al.*, 2001) and Fe^{III} (Warren & Ferris, 1998) adsorb less to cell surfaces at a lower pH. Additionally, (Urrutia Mera *et al.*, 1992) showed that cells of *Bacillus subtilis* bind heavy metals such as U and Sc substantially less to their cell surface when the cells were alive (with a functioning pmf). Less adsorption of metals due to competition with H^+ leads to fewer potential nucleation sites for mineral precipitation (Urrutia Mera *et al.*, 1992; Fein *et al.*, 2001).

The lower pH not only influences the competition of the Fe^{III}_{aq} ions with protons for the cell surface-binding sites, but it also changes the solubility of Fe^{III} itself. Because the concentration of Fe^{III}_{aq} ions and therefore the solubility of the Fe^{III} determine the kinetics and the extent of precipitation (Grundl & Delwiche, 1993; Pham *et al.*, 2006; Rose & Waite, 2007), we determined the effect of a pH change of 0.6

from pH 6.6 to 6.0 on the solubility of Fe^{III} (Fig. 2). Geochemical modeling showed that a lower pH of 6.0, which is present at the cell surface, will increase the fraction of Fe^{III} that is in solution (Fe^{III}_{aq}) approximately fivefold compared with the bulk pH of 6.6, i.e. the concentration of Fe^{III}_{aq} is only 20% at pH 6.6 compared with pH 6.0. Similar to that for chemical Fe^{II} oxidation, probably also during microbial Fe^{II} oxidation, the rate-limiting step in the transition from Fe^{II}_{aq} to Fe^{III}_{ppt} via Fe^{III}_{aq} is the nuclation and precipitation of the Fe^{III} mineral (Grundl & Delwiche, 1993). The precipitation rate of Fe^{III} therefore decreases with decreasing pH. At pH 6.0 (cell), the precipitation rate was determined to be 8.3×10^{-10} mM s^{-1} whereas at pH 6.6 (bulk) the rate increased to 1.3×10^{-9} mM s^{-1}. All in all, equilibrium calculations showed that the Fe^{III}_{aq} concentration is higher at a lower pH. Additionally, precipitation of Fe^{III} minerals in the bulk medium is faster because the pH in the bulk is higher than that at the cell surface. Therefore, a concentration gradient of Fe^{III}_{aq} establishes between the cell surface and the bulk, with a higher Fe^{III}_{aq} concentration at the lower pH at the cell surface and a lower Fe^{III}_{aq} concentration at the higher pH in the bulk medium. The concentration gradient of Fe^{III}_{aq} drives diffusion of Fe^{III}_{aq} from low-pH zones at the cell surface (low precipitation, higher Fe^{III}_{aq}) to high-pH regions further away from the cell (faster precipitation, low Fe^{III}_{aq}, high mineral content) (Fig. 3).

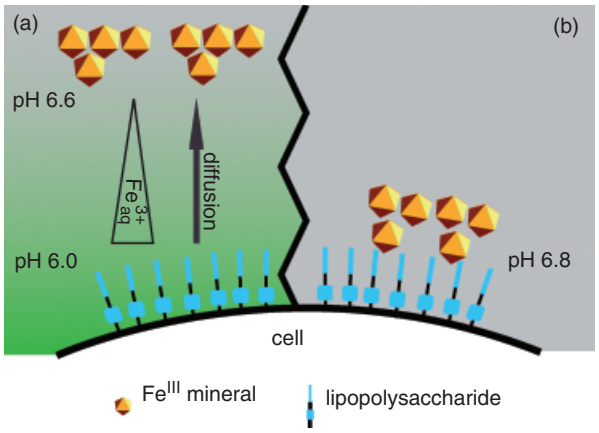

Fig. 3. Scheme of a gram-negative microbial cell interacting with dissolved Fe^{III} species and Fe^{III} minerals. (a) Active metabolism with a pH microenvironment around the cell. Fe^{III} remains in solution in a cell pH microenvironment directing precipitation to the bulk medium. (b) Scenario illustrating Fe^{III} interaction with the cell surface in the absence of a pH microenvironment, with Fe^{III} preferentially binding and precipitating at the cell surface.

Consequences of the low cell surface pH for cell encrustation and metal binding in photoferrotrophs and implications for chemotrophic Fe^{II} oxidizers

In this study, we demonstrated the establishment of a single-cell low-pH microenvironment at the cell surface of the phototrophic Fe^{II}-oxidizer *Thiodictyon* sp. strain F4 using an *in-situ* approach with a pH-dependent fluorescent dye in combination with confocal laser scanning microscopy. The observed pH decrease at the cell surface has three consequences for the cell: (1) a successful competition of protons with the Fe^{III}_{aq} for sorption sites at the cell surface leading to less binding of Fe^{III} to the cell surface, (2) an increase in Fe^{III} solubility and (3) a lower precipitation rate of Fe^{III}_{ppt} at the cell surface (Fig. 3). This suggests that the establishment of a cell pH microenvironment could provide a mechanism for photoferrotrophs to successfully prevent Fe^{III} mineral precipitation on the cell surface. The results of this study may therefore explain why none of the known phototrophic Fe^{II}-oxidizing strains encrusts (Fig. 1). An exception is the purple nonsulfur bacteria, *Rhodomicrobium vannielii*, which differs from the other photoferrotrophs in that it is a mixotrophic Fe^{II} oxidizer, i.e. it needs an organic substrate in addition to the Fe^{II}, and it is not clear whether this strain benefits from Fe^{II} oxidation at all (Heising & Schink, 1998; Schaedler *et al.*, 2009). The benefits for a cell to avoid encrustation are obvious because (1) more light can reach the cell surface, leading to a higher metabolic rate, and (2) the uptake of nutrients from the environment and the release of toxic metabolites to the surrounding is not hampered.

For chemotrophic Fe^{II}-oxidizing strains, other mechanisms to prevent cell encrustation are expected, because these microorganisms depend solely on the energy provided by the chemotrophic oxidation of Fe^{II} with either O_2 or nitrate as electron acceptor. Protons therefore cannot be pumped using light energy as by the phototrophs in cyclic photophosphorylation where a single electron can be used multiple times to pump protons as long as light energy is available. In chemotrophic Fe^{II} oxidizers, proton translocation is directly coupled to chemotrophic Fe^{II} oxidation and electron transport phosphorylation, where one electron stemming from the oxidation of Fe^{II} runs through the electron transport chain once, finally being used to reduce O_2 or nitrate. It has been shown that some nitrate-reducing mixotrophic Fe^{II}-oxidizing bacteria encrust with Fe^{III}_{ppt} on the cell surface (Miot *et al.*, 2009a; Schaedler *et al.*, 2009). Although these bacteria also utilize the PMF to generate ATP and to produce reducing equivalents, the energy available to these bacteria is much less compared with the phototrophic strains because phototrophic organisms can tap the energy source of the solar radiation. In contrast, chemotrophic organisms (such as nitrate-reducing and microaerophilic Fe^{II}-oxidizing bacteria) are limited by the energy that can be obtained from Fe^{II} oxidation, which makes the generation of a large proton gradient less likely or even impossible.

The results presented here shed light on a long lasting enigma: already in 19th century Ehrenberg (1836) and

Winogradsky (1888) had observed biogenic Fe^{III} minerals and speculated on their formation and the influence of bacteria. Although many open questions remain, today, almost 200 years later, we understand the complexity of the interaction between bacteria and the Fe^{III} minerals better. The presence of pH microenvironments around phototrophic Fe^{II} oxidizers provides a possible explanation as to why and how phototrophic Fe^{II}-oxidizing bacteria avoid encrustation by Fe^{III} minerals. Additionally, the light dependence of this metabolism potentially explains why phototrophic Fe^{II} oxidizers use a different strategy to avoid cell encrustation than the microaerophilic Fe^{II}-oxidizing bacteria, such as *Gallionella* and *Leptothrix*.

Acknowledgements

We would like to thank Jürgen Berger for his help with confocal scanning laser microscopy; Sebastian Behrens and Nicole Posth are acknowledged for reading the manuscript and helpful comments. We would also like to thank the University of Tuebingen for partially funding F.H. (Promotionsverbund Grenzflächen), the German Research Foundation (DFG) and the Stifterverband der Wissenschaft for funding A.K. and the Max-Planck Society for supporting H.S. We also thank two anonymous reviewers for their helpful comments, which improved the quality of the manuscript.

References

Barbeau K, Rue EL, Bruland KW & Butler A (2001) Photochemical cycling of iron in the surface ocean mediated by microbial iron(III)-binding ligands. *Nature* **413**: 409–413.

Beveridge TJ & Murray RG (1976) Uptake and retention of metals by cell walls of *Bacillus subtilis*. *J Bacteriol* **127**: 1502–1518.

Beveridge TJ & Murray RG (1980) Sites of metal deposition in the cell wall of *Bacillus subtilis*. *J Bacteriol* **141**: 876–887.

Borrok D, Fein JB, Tischler M, O'Loughlin E, Meyer H, Liss M & Kemner KM (2004) The effect of acidic solutions and growth conditions on the adsorptive properties of bacterial surfaces. *Chem Geol* **209**: 107–119.

Canfield DE, Thamdrup B & Kristensen E (2005) *Aquatic Geomicrobiology*. Elsevier Academic Press, San Diego, CA.

Chan CS, Fakra SC, Edwards DC, Emerson D & Banfield JF (2009) Iron oxyhydroxide mineralization on microbial extracellular polysaccharides. *Geochim Cosmochim Ac* **73**: 3807–3818.

Croal LR, Gralnick JA, Malasarn D & Newman DK (2004a) The genetics of geochemistry. *Annu Rev Genet* **38**: 175–202.

Croal LR, Johnson CM, Beard BL & Newman DK (2004b) Iron isotope fractionation by Fe(II)-oxidizing photoautotrophic bacteria. *Geochim Cosmochim Ac* **68**: 1227–1242.

Croal LR, Jiao Y & Newman DK (2007) The fox operon from *Rhodobacter* strain SW2 promotes phototrophic Fe(II) oxidation in *Rhodobacter capsulatus* SB1003. *J Bacteriol* **189**: 1774–1782.

Ehrenberg CG (1836) Vorläufige Mitteilungen über das wirkliche Vorkommen fossiler Infusorien und ihre große Verbreitung. *Poggendorfs Annalen Physik Chemie* **38**: 213–227.

Ehrlich HL & Newman DK (2009) *Geomicrobiology*. CRC Press, New York.

Emerson D (2000) Microbial Oxidation of Fe(II) and Mn(II) at circumentural pH. *Environmental Microbe–Metal Interactions* (Lovely DR, ed), pp. 31–52. ASM Press, Washington.

Emerson D & Revsbech NP (1994) Investigation of an iron-oxidizing microbial mat community located near Aarhus, Denmark: field studies. *Appl Environ Microb* **60**: 4022–4031.

Fein JB, Martin AM & Wightman PG (2001) Metal adsorption onto bacterial surfaces: development of a predictive approach. *Geochim Cosmochim Ac* **65**: 4267–4273.

Grundl T & Delwiche J (1993) Kinetics of ferric oxyhydroxide precipitation. *J Contam Hydrol* **14**: 71–97.

Hafenbradl D, Keller M, Dirmeier R, Rachel R, Rossnagel P, Burggraf S, Huber H & Stetter KO (1996) *Ferroglobus placidus* gen. nov., sp. nov., A novel hyperthermophilic archaeum that oxidizes Fe^{2+} at neutral pH under anoxic conditions. *Arch Microbiol* **166**: 308–314.

Harold FM (1972) Conservation and transformation of energy by bacterial membranes. *Bacteriol Rev* **36**: 172–230.

Hegler F, Posth N, Jiang J & Kappler A (2008) Physiology of phototrophic iron(II)-oxidizing bacteria – implications for modern and ancient environments. *FEMS Microbiol Ecol* **66**: 250–260.

Heising S & Schink B (1998) Phototrophic oxidation of ferrous iron by a *Rhodomicrobium vannielii* strain. *Microbiology* **144**: 2263–2269.

Invitrogen (2003) *SNARF pH Indicators: User Manual*. Molecular Probes Europe, Invitrogen, Leiden, The Netherlands.

Jiao Y & Newman DK (2007) The pio operon is essential for phototrophic Fe(II) oxidation in *Rhodopseudomonas palustris* TIE-1. *J Bacteriol* **189**: 1765–1773.

Johnson KJ, Ams DA, Wedel AN, Szymanowski JES, Weber DL, Schneegurt MA & Fein JB (2007) The impact of metabolic state on Cd adsorption onto bacterial cells. *Geobiology* **5**: 211–218.

Kappler A & Newman DK (2004) Formation of Fe(III)-minerals by Fe(II)-oxidizing photoautotrophic bacteria. *Geochim Cosmochim Ac* **68**: 1217–1226.

Marcotte N & Brouwer AM (2005) Carboxy SNARF-4F as a fluorescent pH probe for ensemble and fluorescence correlation spectroscopies. *J Phys Chem B* **109**: 11819–11828.

Martinez RE, Gardés E, Pokrovsky OS, Schott J & Oelkers EH (2010) Do photosynthetic bacteria have a protective mechanism against carbonate precipitation at their surfaces? *Geochim Cosmochim Ac* **74**: 1329–1337.

McConnaughey TA & Whelan JF (1997) Calcification generates protons for nutrient and bicarbonate uptake. *Earth-Sci Rev* **42**: 95–117.

Miot J, Benzerara K, Morin G *et al.* (2009a) Iron biomineralization by neutrophilic iron-oxidizing bacteria. *Geochim Cosmochim Ac* **73**: 696–711.

Miot J, Benzerara K, Obst M, Kappler A, Hegler F, Schaedler S, Bouchez C, Guyot F & Morin G (2009b) Extracellular iron biomineralization by photoautotrophic iron-oxidizing bacteria. *Appl Environ Microb* **75**: 5586–5591.

Mitchell P (1979) Keilin's respiratory chain concept and its chemiosmotic consequences. *Science* **206**: 1148–1159.

Nicholls DG & Ferguson SJ (2002) *Bioenergetics*, *Vol. 3*. Academic Press, Amsterdam.

Padan E, Zilberstein D & Schuldiner S (1981) pH homeostasis in bacteria. *Biochim Biophys Acta* **650**: 151–166.

Pham AN, Rose AL, Feitz AJ & Waite TD (2006) Kinetics of Fe(III) precipitation in aqueous solutions at pH 6.0–9.5 and 25 degrees C. *Geochim Cosmochim Ac* **70**: 640–650.

Rose AL & Waite TD (2007) Reconciling kinetic and equilibrium observations of iron(III) solubility in aqueous solutions with a polymer-based model. *Geochim Cosmochim Ac* **71**: 5605–5619.

Schaedler S, Burkhardt C & Kappler A (2008) Evaluation of electron microscopic sample preparation methods and imaging techniques for characterization of cell–mineral aggregates. *Geomicrobiol J* **25**: 228–239.

Schaedler S, Burkhardt C, Hegler F, Straub KL, Miot J, Benzerara K & Kappler A (2009) Formation of cell–iron–mineral aggregates by phototrophic and nitrate reducing anaerobic Fe(II)-oxidizing bacteria. *Geomicrobiol J* **26**: 93–103.

Sobolev D & Roden EE (2001) Suboxic deposition of ferric iron by bacteria in opposing gradients of Fe(II) and oxygen at circumneutral pH. *Appl Environ Microb* **67**: 1328–1334.

Straub KL, Benz M, Schink B & Widdel F (1996) Anaerobic, nitrate-dependent microbial oxidation of ferrous iron. *Appl Environ Microb* **62**: 1458–1460.

Stumm W & Morgan JJ (1995) *Aquatic Chemistry: Chemical Equilibria and Rates in Natural Waters*. Wiley-Interscience, New York.

Urrutia Mera M, Kemper M, Doyle R & Beveridge TJ (1992) The membrane-induced proton motive force influences the metal binding ability of Bacillus subtilis cell walls. *Appl Environ Microb* **58**: 3837–3844.

Warren LA & Ferris FG (1998) Continuum between sorption and precipitation of Fe(III) on microbial surfaces. *Environ Sci Technol* **32**: 2331–2337.

Widdel F, Schnell S, Heising S, Ehrenreich A, Assmus B & Schink B (1993) Ferrous iron oxidation by anoxygenic phototrophic bacteria. *Nature* **362**: 834–836.

Winogradsky S (1888) Ueber Eisenbacterien. *Botanische Zeitung* 261–270.

Yee N & Fein JB (2003) Quantifying metal adsorption onto bacteria mixtures: a test and application of the surface complexation model. *Geomicrobiol J* **20**: 43–60.